Phase transitions between polytypes and intralayer superstructures in transition metal dichalcogenides

H. Katzke,[1,*] P. Tolédano,[1,2] and W. Depmeier[1]
[1]*Institute of Geosciences, Crystallography, University of Kiel, Olshausenstraße 40, 24098 Kiel, Germany*
[2]*Groupe "Structure des Matériaux sous conditions extrêmes" SNBL/ESRF, Boîte Postale 220, 38043 Grenoble Cedex, France*
(Received 28 November 2003; published 22 April 2004)

The different polytypic structures observed in transition metal dichalcogenides are described as the result of ordering processes from a common parent disordered polytype structure. Interpolytypic transitions are suggested to be favored by the intrinsic stacking faults induced in the ordering mechanisms. The influence of these mechanisms on the intralayer superstructures is discussed.

DOI: 10.1103/PhysRevB.69.134111 PACS number(s): 64.70.Kb, 81.30.Kf

I. INTRODUCTION

Since the observation of stacking disorder in molybdenum and niobium disulphides by Jellinek, Brauer, and Müller,[1] the transition metal dichalcogenides (TMD's) have attracted considerable interest from a number of viewpoints,[2–4] including intercalation physics, charge-density waves, superconductivity, and optical and transport properties. The common thread that ties these properties together is the pseudo-two-dimensional nature of the materials, which are structurally similar in that they are all made up of *X-M-X* slabs where *X* refers to a chalcogen (S, Se, Te) and *M* is a transition metal belonging to group IVb (Ti, Zr, Hf), group Vb (V, Nb, Ta), or group VIb (Cr, Mo, W). TMD's display strong intralayer covalent bonding and weak interlayer van der Waals bonding. Sheets of *M* atoms are strongly bonded and sandwiched each between two hexagonal close-packed layers of *X* atoms, the coordination of *M* atoms being either octahedral or trigonal-prismatic. The MX_2 slabs are weakly bonded and stacked along the direction perpendicular to the layers. Various stacking sequences give rise to polytypism. The basic symmetries of TMD's are either hexagonal or rhombohedral.

In the present work, we intend to go beyond the observation of similarities between the various TMD structures, and to describe the different atomistic mechanisms which relate these structures to a common disordered parent structure. The mechanisms are described as ordering processes similar to those which connect the phases surrounding an order-disorder phase transition. After describing crystallographically the ordering process for each type of polytype structure (Sec. II A), we show that these processes correspond to a small number of order-parameter symmetries and basic phase diagrams (Sec. II B). They also imply intrinsic stacking faults when the temperature is varied. This provides a justification for the interpolytypic transitions found in TMD materials. The influence of the polytypic ordering on the commensurate and incommensurate superstructures reported in members of the TMD family is discussed in Sec. III.

II. THEORY OF INTERPOLYTYPIC PHASE TRANSITIONS IN TRANSITION METAL DICHALCOGENIDES

A. Crystallographic description

Eleven different types of polytype structures have been observed up to now in TMD materials[2] which are represented schematically in Fig. 1. Their occurrence among the TMD materials is indicated below each polytype structure. On top of Fig. 1, a hypothetic structure formed by one MX_2 layer is shown which will be assumed in our description to be the *disordered parent structure* for all the *ordered* MX_2 polytypes. In this structure, which has the hexagonal $P6/mmm$ symmetry and will be denoted hereafter as the *P* structure, the *M* and *X* atoms are statistically disordered with a fractional occupancy $x_M = x_X = 1/3$ corresponding to one formula unit MX_2 per primitive hexagonal cell. The *M* atoms occupy statistically the positions $1(b)$: 0 0 1/2 and $2(d)$: 1/3 2/3 1/2, whereas the *X* atoms are disordered over the Wyckoff positions $2(e)$: 0 0 *z* and $4(h)$: 1/3 2/3 *z* with *z* close to $z_0 = 1/4$. We will now describe the ordering mechanisms which lead to the formation of the MX_2 polytypes in order of increasing complexity using the Ramsdell notation[5] nY for the stacking polytypic sequences, where *n* is the number of *X-M-X* slabs in a unit cell and *Y* stands for the lattice type which can be trigonal (T), hexagonal (H), or rhombohedral (R).

1. 1T polytype

The only known structure with one MX_2 layer per unit cell is that of the $1T$ polytype, which is found for all group IVb and vanadium dichalcogenides and for TaS_2, $TaSe_2$, NbS_2, and $NbSe_2$.[2] This structure is obtained when the *M* atoms order on the $1(b)$ position and the *X* atoms occupy half of the $4(h)$ positions. The parent hexagonal symmetry is lowered to $P\bar{3}m1$ with the octahedrally coordinated *M* atoms in $1(a)$ positions, and the *X* atoms in $2(d)$ positions. The layer stacking is of the CbA type where capital letters correspond to the chalcogen positions and lower case letters designate the *M* positions.

2. 2H polytypes

Three different polytypes are known to possess two MX_2 layers per unit cell which are denoted $2H_a$, $2H_b$, and $2H_c$. Dichalcogenides of Nb and Ta crystallize in the $2H_a$ structure whereas the $2H_c$ polytypes are stabilized in Mo and W dichalcogenides. The $2H_b$ polytypes are obtained for the nonstoichiometric compounds $Nb_{1+x}Se_2$ and $Ta_{1+x}Se_2$, with the excess metal atoms intercalated in the van der Waals interlayer gaps. All three polytypes involve a doubling of the

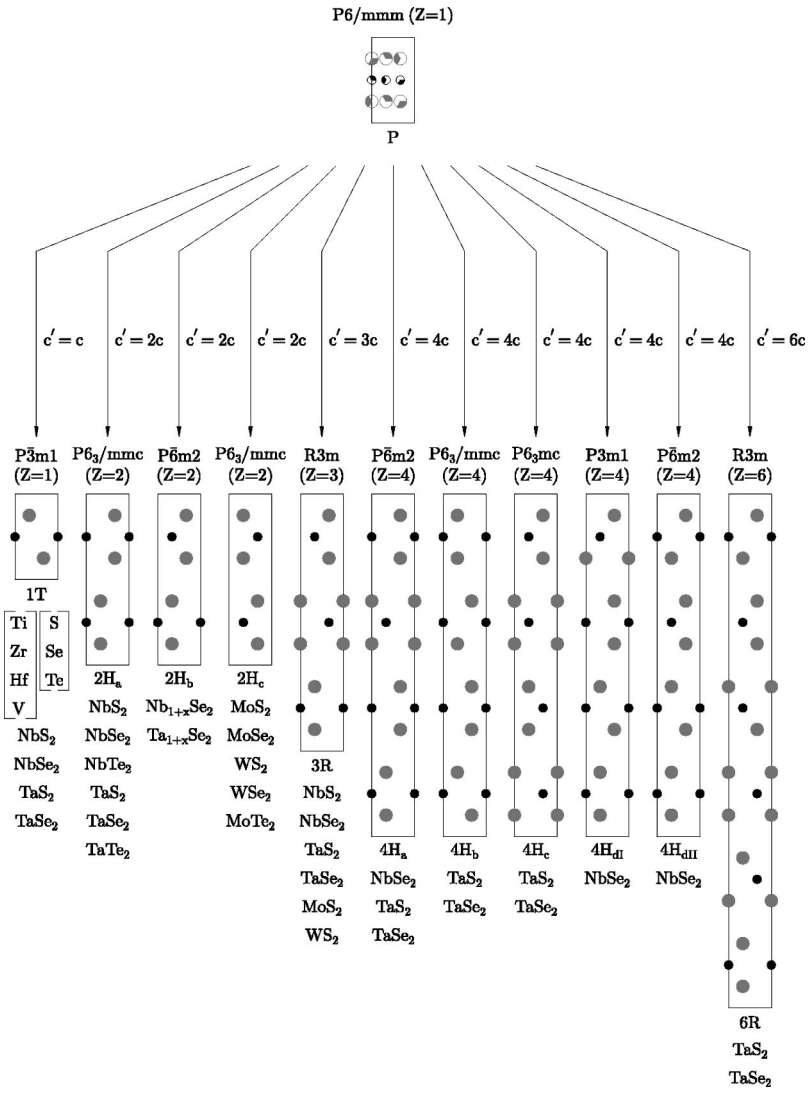

FIG. 1. Ordering mechanisms leading to the formation of the 11 polytype structures observed in TMD materials. The polytypes are shown as $(11\bar{2}0)$ projections of their hexagonal structures. Small circles represent the metal atoms and large circles the chalcogens. The partial filling of the circles for the *P* structure indicates the positional occupancy.

c-lattice translation with respect to the *P* structure, corresponding to one $2(e)$ and one $4(h)$ position for the *M* atoms. Each of the *X* positions $2(e)$ and $4(h)$ in the *P* structure split into two $2(e)$ and two $4(h)$ positions. A further ordering mechanism yields a differentiation between the $2H$ polytypes.

(i) In the $2H_a$ polytype the *M* atoms occupy the $2(e)$ position whereas the *X* atoms fill the two $4(h)$ positions, one half each. The resulting structure has $P6_3/mmc$ symmetry, in which the *M* atoms occupy the $2(b)$ positions (0 0 1/4) and the *X* atoms the positions $4(f)$: 1/3 2/3 *z* with $z \sim 1/8$. The corresponding stacking sequence is $AbACbC$.

(ii) In the $2H_b$ polytype the position $2(e)$ is half filled and the position $4(h)$ is filled by one-quarter with *M* atoms. The chalcogens are shared between the two initial $4(h)$ positions. The parent hexagonal symmetry is reduced to $P\bar{6}m2$ with the positions $1(a)$ and $1(d)$ for the *M* atoms and the position $2(h)$: 1/3 2/3 *z* and $2(i)$: 2/3 1/3 *z* for the *X* atoms. The stacking sequence is $AbACaC$.

(iii) In the $2H_c$ polytype, half of the $4(h)$ position is filled by the metal atoms whereas the *X* atoms occupy half of the two $4(h)$ positions. The space-group type is $P6_3/mmc$, as for the $2H_a$ polytype. However, since the metal atoms occupy the positions $2(c)$: 1/3 2/3 1/4, and the chalcogens the positions $4(f)$: 1/3 2/3 *z*, the *M* atoms in adjacent layers are displaced by 1/3 2/3 0 with respect to their positions in the $2H_a$ structure where they are on top of each other. The stacking sequence is $CaCAcA$.

3. 3R polytype

The $3R$ polytype structure with the rhombohedral $R3m$ polar symmetry has been observed in NbS_2, $NbSe_2$, TaS_2, $TaSe_2$, MoS_2, and WS_2. Its three-layer structure corresponds to a triplication of the parent *c* translation and a consecutive ordering of the *M* and *X* atoms over the available positions. The triplication of the *P* unit cell leads to a splitting of the $1(b)$ metal atom positions into nonequivalent $1(b)$ and $2(e)$ positions, while the $2(d)$ metal atom positions split into $2(d)$ and $4(h)$. Each of the initial $2(e)$ and $4(h)$ chalcogen positions splits into three different $2(e)$ and $4(h)$ positions. In the $3R$ polytype, half of the $2(e)$ and $2(d)$ positions and one-quarter of the $4(h)$ position are filled by the metal atoms. The chalcogens occupy the $2(e)$ position and two of the $4(h)$ positions half. In the ordered rhombohedral struc-

TABLE I. Change in the Wyckoff positions from the P structure to the $4H_a$, $4H_b$, $4H_c$, $4H_{dI}$, and $4H_{dII}$ polytypes, and stacking sequences.

Polytype	Initial Wyckoff positions in the P structure	Final Wyckoff positions	Stacking sequences
$4H_a$	M:$[2(e)]$,$[2(e)]_{1/2}$,$[4(h)]_{1/4}$, X:$[2(e)]_{1/2}$,$[2(e)]_{1/2}$,$[4(h)]_{1/2}$,$[4(h)]_{1/2}$,$[4(h)]_{1/4}$, X:$[4(h)]_{1/4}$	M:1(a),1(d),2(g), X:2(g),2(h),2(i),2(i)	*AbA CbC BaB CbC*
$4H_b$	M:$[2(e)]$,$[2(e)]$, X:$[4(h)]_{1/2}$,$[4(h)]_{1/2}$,$[4(h)]_{1/2}$,$[4(h)]_{1/2}$	M:2(a),2(b), X:4(f),4(f)	*CbA CbC AbC AbA*
$4H_c$	M:$[4(h)]_{1/2}$,$[4(h)]_{1/2}$, X:$[2(e)]_{1/2}$,$[2(e)]_{1/2}$,$[2(e)]_{1/2}$,$[2(e)]_{1/2}$,$[4(h)]_{1/4}$, X:$[4(h)]_{1/4}$,$[4(h)]_{1/4}$,$[4(h)]_{1/4}$	M:2(b),2(b), X:2(a),2(a),2(b),2(b)	*BcB AcA BaB CaC*
$4H_{dI}$	M:$[2(e)]$,$[2(e)]_{1/2}$,$[4(h)]_{1/4}$, X:$[2(e)]_{1/2}$,$[4(h)]_{1/2}$,$[4(h)]_{1/2}$,$[4(h)]_{1/2}$,$[4(h)]_{1/4}$	M:1(a),1(a),1(a),1(b), X:1(a),1(b),1(b),1(b),1(c),1(c),1(c),1(c)	*AbA CbA CbC BaC*
$4H_{dII}$	M:$[2(e)]$,$[2(e)]_{1/2}$,$[4(h)]_{1/4}$, X:$[4(h)]_{1/2}$,$[4(h)]_{1/2}$,$[4(h)]_{1/2}$,$[4(h)]_{1/2}$	M:1(a),1(d),2(g), X:2(h),2(h),2(i),2(i)	*AbA CbA CaC AbC*

ture both metal atoms and chalcogens are in positions $3(a)$: 0 0 z, with $z\sim 0$ for the M atoms while for the X atoms $z \sim 1/4$ and $z\sim 5/12$. The stacking sequence is $AbABcBCaC$.

4. 4H polytypes

Five different polytypes with four slabs per unit cell have been observed in TMD's.[1,2] They are shown schematically in Fig. 1. The polytypes $4H_a$, $4H_b$, and $4H_c$ are obtained at different temperatures in TaS_2 and $TaSe_2$, whereas the polytypes $4H_a$, $4H_{dI}$, and $4H_{dII}$ form in $NbSe_2$. In the $4H_a$ and $4H_c$ structures the metal atoms are exclusively in trigonal-prismatic coordination, while they display mixed octahedral and trigonal-prismatic coordination in the $4H_b$, $4H_{dI}$, and $4H_{dII}$ structures. Table I indicates the changes in the Wyckoff positions from the disordered P structure to the final ordered structures as well as the corresponding stacking sequences. The ordering process reduces the parent symmetry to $P\bar{6}m2$ ($4H_a$, $4H_{dII}$), $P6_3/mmc$ ($4H_b$), $P6_3mc$ ($4H_c$), and $P3m1$ ($4H_{dI}$).

5. 6R polytype

The $6R$ polytype with $R3m$ symmetry is observed in TaS_2 and $TaSe_2$. Half of the M atoms of the six-layer structure are octahedrally coordinated, while the other half are in trigonal-prismatic coordination. The sixfold multiplication of the P unit cell causes a splitting of the $1(b)$, $2(d)$, $2(e)$, and $4(h)$ positions into, respectively, three $2(e)$ and $4(h)$ positions and six $2(e)$ and $4(h)$ positions. The ordering mechanism producing the $6R$ structure consists of a filling by the M atoms of one of the $2(e)$ positions and a half filling of two of the $4(h)$ positions. The X atoms occupy one of the $2(e)$ positions fully and two of the six $2(e)$ positions one half each. From the six $4(h)$ positions, three are half filled and two are occupied at one-quarter by X atoms. In the final $R3m$ structure all atoms occupy the $3(a)$: 0 0 z positions. The $6R$ stacking sequence is $AbABcABcBCaBCaCAbC$.

B. Order-parameter symmetries, free energies, and phase diagrams

From the translational symmetry breaking occurring in the transition from the P structure to the ordered polytype structures, indicated in Fig. 1, one can deduce that all these latter structures are related to instabilities corresponding to points of the hexagonal Brillouin zone (BZ) located on the Δ (Γ-A) line. Using Kovalev's notation[6] for the irreducible representations (IREPS) of the $P6/mmm$ space group, a Landau-type symmetry analysis[7] yields the following description, summarized in Fig. 2.

(1) The $P\rightarrow 1T$ phase transition is induced by the one-dimensional IREP $\tau_5(k_{16})$ of the BZ center (Γ point), the symmetry breaking order parameter η coinciding with the elastic stiffness component C_{14}. The order-parameter expansion has the canonical form

$$F_1(T,P,\eta)=F_{01}(T,P)+\frac{\alpha_1}{2}\eta^2+\frac{\beta_1}{4}\eta^4+\frac{\gamma_1}{6}\eta^6+\cdots. \tag{1}$$

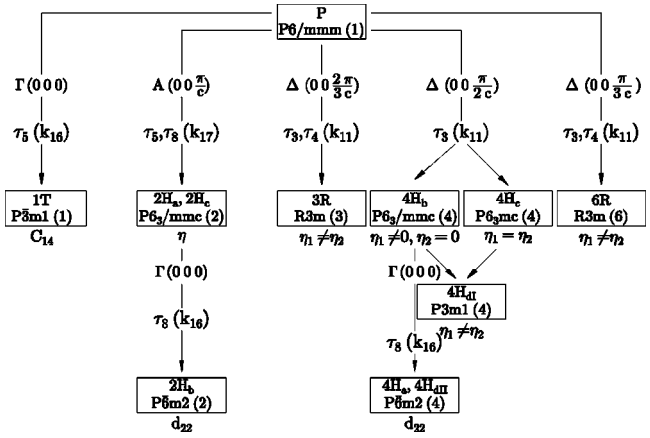

FIG. 2. Order-parameter symmetries for the ordering transitions from the P structure to the ordered polytypes. The points of the hexagonal Brillouin zone and the irreducible representations (in Kovalev's notation[6]) are indicated. The macroscopic tensor components arising at the transitions (C_{14}, d_{22}) and the equilibrium relationships fulfilled by the order-parameter components η_i are indicated below each polytype. The IREP denoted $\tau_3(k_{11})$ corresponds to the different image groups for the polytypes $3R$ or $6R$ (image group C_{6v}) and $4H_b$ or $4H_c$ (image group C_{4v}) since the respective values of k_z are different.

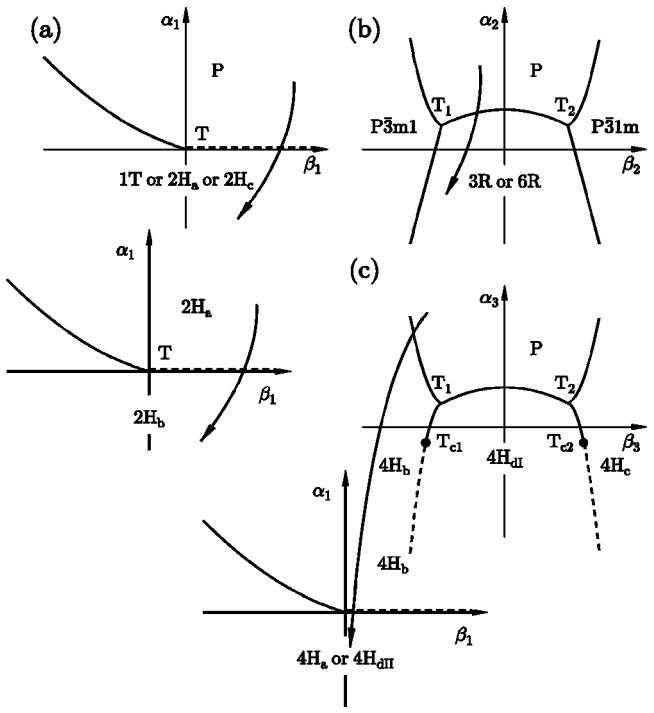

FIG. 3. Basic topological features of the phase diagrams involving the P phase and the different polytype structures. Dashed and full lines represent second- and first-order transition lines, respectively. T_1 and T_2 are triple points. T, T_{c1}, and T_{c2} are tricritical points. The arrows represent possible thermodynamic paths, showing that the $2H_b$, $4H_a$, and $4H_{dII}$ structures cannot be reached directly from the P phase.

The standard phase diagram associated with F_1 is represented in Fig. 3(a). It involves a first-order ($\beta_1<0$) or second-order ($\beta_1>0$) $P\rightarrow 1T$ transition.

(2) The $P\rightarrow 2H_a$ and $P\rightarrow 2H_c$ transitions result from the activation of a one-dimensional IREP [$\tau_5(k_{17})$] at the boundary A point of the hexagonal BZ. The order-parameter expansion has the same form as given in Eq. (1) and therefore the transition corresponds to the same phase diagram as in Fig. 3(a). In contrast, the $2H_b$ structure cannot be obtained directly from the P structure, but only via the $2H_a$ structure. This is consistent with the observation that in TMD compounds (as $TaSe_2$ or $NbSe_2$) the $2H_b$ and $2H_a$ polytypes always take place concomitantly, the $2H_b$ structure stabilizing at lower temperature. The $2H_a\rightarrow 2H_b$ transition is induced by a zone-center instability of the $P6_3/mmc$ space group [$\tau_8(k_{16})$] giving rise to a spontaneous component (d_{22}) of the piezoelectric tensor.

(3) The $3R$, $4H$, and $6R$ symmetries are related to bidimensional IREPS of $P6/mmm$, corresponding to points located on the Δ line ($0\ 0\ k_z$) of the hexagonal BZ, with $k_z=2\pi/3c$ ($3R$), $k_z=\pi/2c$ ($4H$), and $k_z=\pi/3c$ ($6R$). The $P\rightarrow 3R$ and $P\rightarrow 6R$ transition order-parameter symmetry has the image group C_{6v} which is the group formed by the distinct matrices of the IREP,[7] with the equilibrium values of the order-parameter components $\eta_1\neq 0, \eta_2\neq 0$. Using the polar mapping $\eta_1=\rho\cos\Theta$ and $\eta_2=\rho\sin\Theta$, the Landau free energy reads

$$F_2(T,P,\rho,\Theta)=F_{02}(T,P)+\frac{\alpha_2}{2}\rho^2+\frac{\beta_2}{4}\rho^4+\frac{\gamma_2}{6}\rho^6+\frac{\gamma_2'}{6}\rho^6\cos 6\Theta+\cdots. \quad (2)$$

Note that the $R3m$ symmetry of the $3R$ and $6R$ structures corresponds to a limit situation which is reached for specific positions of the atoms [$(0\ 0\ z)$, $(1/3\ 2/3\ 2/3+z)$, and $(2/3\ 1/3\ 1/3+z)$] of the $P3m1$ supergroup symmetry which is actually induced by the IREP $\tau_3(k_{11})$ of $P6/mmm$. It has the consequence that the phase transitions to the limit states $3R$ and $6R$ from the other polytype polymorphs are of the reconstructive type (the group-subgroup relationship being lost) and, in particular, are necessarily first order as assumed in the phase diagram of Fig. 3(b).

The $P\rightarrow 4H_b$, $P\rightarrow 4H_c$, and $P\rightarrow 4H_{dI}$ transitions correspond to a different order-parameter symmetry with the image group C_{4v} associated with the free energy

$$F_3(T,P,\rho,\Theta)=F_{03}(T,P)+\frac{\alpha_3}{2}\rho^2+\frac{\beta_3}{4}\rho^4+\frac{\beta_3'}{4}\rho^4\cos 4\Theta+\cdots. \quad (3)$$

The $4H_b$ and $4H_c$ structures are stabilized when $\eta_1\neq 0$, $\eta_2=0$ and $\eta_1=0$, $\eta_2\neq 0$, respectively, whereas the $4H_{dI}$ structure occurs for $\eta_1\neq 0$ and $\eta_2\neq 0$. The $4H_a$ and $4H_{dII}$ structures cannot be obtained directly from the P structure but derive from the $4H_b$ structure, being induced by the zone-center instability $\tau_8(k_{10})$ of the $P6_3/mmc$ space group. Figure 3(c) shows the theoretical phase diagram in which the different $4H$ polytypes are inserted.

In TMD materials the $1T$ polytype is generally stable at higher temperatures (e.g., above 950 °C in $TaSe_2$ and $NbSe_2$) and the $2H$ phases at lower temperatures (e.g., 600 °C in $TaSe_2$), while the other polytypes ($3R$, $6R$, $4H$) occur in the intermediate range. Referring to our description, it means that the **k** vector associated with the onset of the polytypes from the P structure *increases* with *decreasing* temperatures from the center (Γ) to the boundary (A point) of the hexagonal Brillouin zone and locks in at the intermediate values $2\pi/3c$, $\pi/2c$, $\pi/3c$ on the Δ line. However, such a picture is oversimplified since the polytypes can stabilize at various temperatures depending on the transformation kinetics and on the treatment of the material (quenching, annealing, slow-cooling or heating, etc.). Figure 4 shows, for example, the interpolytypic transformations observed in $TaSe_2$ under various external conditions.[8–11] One can verify that the transformations are liable to occur between most of the polytypes without simple symmetry constraints such as a group-subgroup relationship between the polytypes, or an increase of their stacking order. This suggests, as noted by Jellinek,[12] that *stacking faults should play an essential role in the interpolytypic transformation mechanisms*.

The existence of a parent disordered polytype structure assumed in our approach implies indeed that the different TMD polytypes should be intrinsically faulted. There are two different origins for the stacking faults.

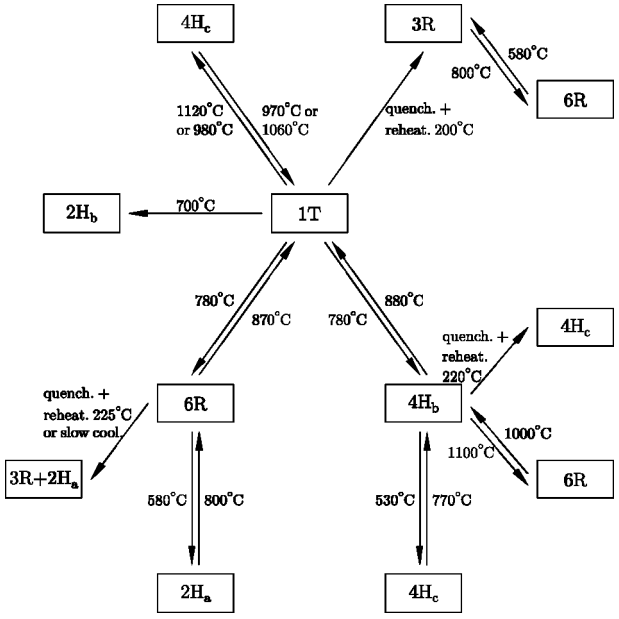

FIG. 4. Interpolytypic phase transitions observed in $TaSe_2$ under different external conditions, from Refs 8–11.

(1) One type of stacking faults results from the lowering of symmetry taking place in the formation of the polytypes from the *P* structure. It gives rise on the one hand to a breaking of translational symmetry corresponding to the existence of *antiphase domains*. Thus, the $2H$, $3R$, $4H$, and $6R$ polytypes should display, respectively, 2, 3, 4, and 6 distinct antiphase domains. These so-called ''deformation'' stacking faults[13] combine with the ''twinning'' stacking faults[13] induced, on the other hand, by the breaking of rotational symmetry ($6/mmm$) of the *P* structure yielding the point subgroups of order 2 ($1T$, $2H_b$, $4H_a$, $4H_c$, and $4H_{dII}$) or 4 ($3R$, $6R$, and $4H_{dI}$).

(2) Another type of stacking faults, which does not depend on symmetry but on temperature, originates in the ordering mechanism assumed for the formation of the TMD polytypes. In the disordered *P* structure each MX_2 slab represents a stacking fault. The ordering process can be characterized by the number $n=1-N_d/N$, where N is the total number of layers and N_d is the number of stacking faults. One has $n=0$ in the *P* structure and $n=1$ in an ideal ordered structure. Intermediate states correspond to $0<n<1$. The value of n at a given temperature is determined by the number of defects. In the ordered structures the asymptotic values of n will reflect the symmetry-induced type of stacking faults, whereas in the disordered structure n accounts as well for the temperature-dependent defects.

From the preceding description one can infer a qualitative picture of the formation of TMD polytypes. Below the melt temperature the polytypes are partially ordered ($0<n<1$) and principally formed by the smaller $1T$ polytypes surrounded by disordered sequences of *P* type polytypes. On cooling the fraction of disordered sequences of layers reduces and the intrinsically faulted regions tend to coalesce, giving rise to longer sequences of ordered polytypes. This picture provides on the one hand a justification, in terms of the interpolytypic transformation kinetics, of the hexagonal *P* structure, assumed from symmetry considerations to be the parent structure for the TMD polytypes. On the other hand it allows us to understand why at moderate or high temperatures a crossover between the different polytypes can occur, as this is favored by a high density of stacking faults.

III. INFLUENCE OF THE LAYER ORDERING ON THE INTRALAYER SUPERSTRUCTURES

Because of their layer structures and weak interlayer interactions TMD materials have been categorized as two-dimensional solids with respect to their in-layer properties. This low dimensionality shows up in many ways as, for example, in the compressibility, optical, electrical and magnetic properties, superconductivity, etc. Along this line most of the models which attempted to describe the intralayer structural phase transitions[14–16] taking place in different polytypes of TMD compounds, such as TaS_2 or $TaSe_2$, have neglected the interpolytypic transitions considered in the preceding section. However, both interlayer and intralayer phase transitions can be observed concurrently (as, for example, in $1T$-$TaSe_2$[2]) and, more generally, there exist several experimental facts showing the influence of the layer stacking on the commensurate and incommensurate superstructures arising at low temperatures within the layers. A coupling between the interlayer and intralayer orderings is obvious for the shortest $1T$ polytypes in which the commensurate superstructures display a three-dimensional character, i.e., $2a\times2a\times2c$ in $1T$-$TiSe_2$, $\sqrt{13}a\times\sqrt{13}a\times13c$ in $1T$-$TaSe_2$, $\sqrt{13}a\times\sqrt{13}a\times3c$ in $1T$-TaS_2, and $4a\times4a\times4c$ in $1T$-VSe_2. For example, in $1T$-TaS_2 the *X*-ray observations by Tanda *et al.*[17] reveal a correlation length corresponding to about 56 layers with a disordering of the layers leading to the stabilization of a triclinic phase (the *T* phase) with a seven-layer periodicity above the commensurate phase.

Although it is less pronounced for the longer polytypes, the influence of the stacking order on the intrapolytypic transitions manifests itself in different ways. For example, in $4H_b$-$TaSe_2$ Lüdecke *et al.*[18] have shown that the location of the charge-density waves in the lock-in superstructure $\sqrt{13}a\times\sqrt{13}a\times c$ is disordered between different layers: the atoms in the Se planes display a transversal modulation along the *c* axis corresponding to a relaxation of these planes to the modulation of the Ta planes. In $2H_a$-$TaSe_2$ one needs to take into account the interlayer coupling in order to describe theoretically the stabilization of a commensurate phase with $Cmcm$ symmetry,[19] or the reentrance under pressure[20] and anisotropy of the discommensurations[21] observed for the preceding phase. Indeed, interlayer interactions have been included in some theoretical approaches to the structural transitions occurring in some of the TMD polytypes as a correction to the discrepancies of the experimental results with single layer models, but the interactions have been restricted to the neighboring layers.

The sequences of commensurate and incommensurate superstructures taking place in the $1T$, $2H_a$, and $4H_b$ polytypes of TMD compounds have been the subject of comprehensive theoretical descriptions[22–27] in the framework of the

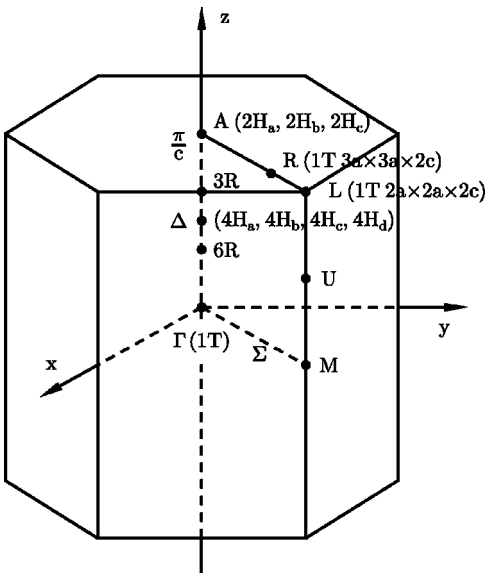

FIG. 5. The hexagonal Brillouin zone with the points and lines involved in the present study.

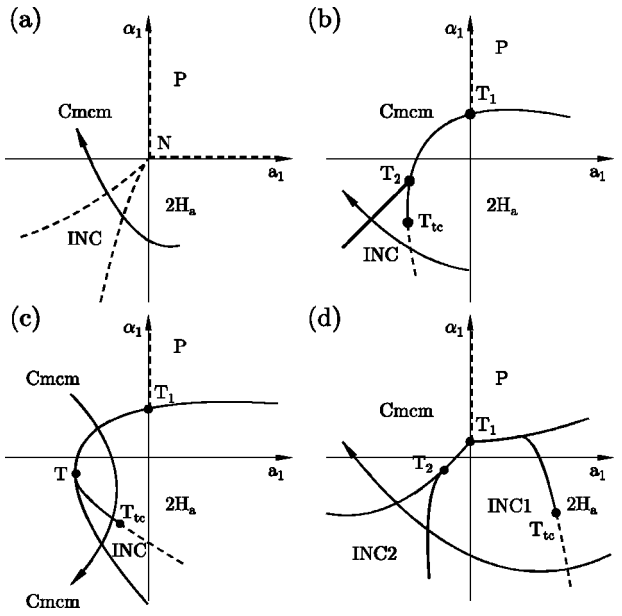

FIG. 6. Phase diagrams resulting from the minimization of the Landau free energy corresponding to the free-energy density given by Eq. (7). Dashed and solid lines correspond to second- and first-order transition lines, respectively. T, T_1, and T_2 are triple points, N is a four-phase point, and T_{tc} is a tricritical point. F_1 is expanded at the sixth degree in η whereas F_4^h corresponds to a sixth degree in ρ in (a)–(c), and to an eighth degree in (d). F_4^{inh} is expanded to the second degree in ρ in (a)–(c) and to the fourth degree in (d). The following conditions distinguish the phase diagrams. (a) $\delta>0$, $\beta_1>0$, $\gamma_1>0$, $b_1+b_2>0$, $c_i>0$, $d_i>0$, $\Delta=4\beta_2 b_2-\delta^2>0$. (b) $\delta>0$, $\beta_1<0$, $\gamma_1>0$, $b_1+b_2>0$, $\Delta>0$, $c_i>0$, $d_i>0$. (c) $\delta>0$, $\beta_1<0$, $\gamma_1>0$, $b_1+b_2<0$, $\Delta>0$, $c_i>0$, $d_i>0$. (d) $\delta>0$, $\beta_1<0$, $\gamma_1>0$, $b_1+b_2<0$, $c_i>0$, $d_i<0$.

Landau theory of phase transitions. In what follows we restrict ourselves to describe the phase diagrams which can be worked out for the illustrative example of the $2H_a$ polytypes, when assuming a full coupling between the stacking order and the in-layer commensurate superstructures. The more complex situations found in $1T$ and $4H_b$ polytypes are only briefly discussed.

The orthorhombic $Cmcm$ commensurate phase found in $2H_a$-$TaSe_2$ below 90 K displays a $3a\times3a\times c$ superstructure, where c is the lattice parameter of the $2H_a$ polytype unit cell. The $P6_3/mmc\rightarrow Cmcm$ structural change, which has been analyzed by Dvořak and Janovec[28] within a standard Landau approach, is associated with the critical wave vector $\mathbf{k}_0=\mathbf{a}^*/3$, where $\mathbf{a}^*=(8\pi/3a,4\pi/3a,0)$ is the basic hexagonal reciprocal lattice vector. $\mathbf{k}_0$ is located along the Σ line, inside the hexagonal Brillouin zone (Fig. 5). Assuming a parent P structure, the superstructure corresponds to $3a\times3a\times2c$, where c is the lattice parameter of the P unit cell, induced by the critical wave vector $\mathbf{k}_c=(\mathbf{a}^*/3,0,\mathbf{c}^*/2)$ ending on the R line of the surface of the hexagonal Brillouin zone ($\mathbf{k}_7$ in Kovalev's notation[6]) (Fig. 5). The little group of $\mathbf{k}_c$ is $G_{k_c}=mm2$ corresponding to a six-branch star $\mathbf{k}_c^*$, which allows the construction of four six-dimensional IREPS of $P6/mmm$, denoted $\tau_1(\mathbf{k}_7)$ to $\tau_4(\mathbf{k}_7)$. A symmetry analysis shows that the $P6/mmm\rightarrow Cmcm$ transition is associated with the IREP denoted $\tau_2(\mathbf{k}_7)$ corresponding to a six-component order parameter formed by the components ζ_i $(i=1-3)$ and their complex conjugate $\zeta_{i+3}=\zeta_i^*(i=1-3)$. Using the polar mapping $\zeta_i=\rho_i\cos\Theta_i$, $\zeta_i^*=\rho_i\sin\Theta_i$ $(i=1-3)$, one can show that the $Cmcm$ structure is stabilized for the equilibrium values of $\rho_1\neq0$, $\rho_2=\rho_3\neq0$, $\Theta_1=(0,\pi)$, and $\Theta_2=\Theta_3=(0,\pi)$. It yields the *effective* form of the Landau free-energy density associated with the $P6/mmm\rightarrow Cmcm$ transition:

$$F_4(T,P,\rho_i,\Theta_i)=F_4^h+F_4^{inh} \tag{4}$$

$$\text{with}\quad F_4^h=F_{04}(T,P)+\frac{a_1}{2}(\rho_1^2+2\rho_2^2)+\frac{b_1}{4}(\rho_1^2+2\rho_2^2)^2+\frac{b_2}{4}(\rho_1^4+2\rho_4^4)+\cdots \tag{5}$$

$$\text{and}\quad F_4^{inh}=\sum_{\substack{i=1,2\\u=x,y}}\left\{c_i\rho_i\frac{d\Theta_i}{du}+d_i\left[\left(\frac{d\rho_i}{du}\right)^2+\rho_i^2\left(\frac{d\Theta_i}{du}\right)^2\right]\right\}+\cdots, \tag{6}$$

where the homogeneous and inhomogeneous parts of the free-energy density have been expanded to the lowest degree involving a symmetry breaking mechanism, i.e., up to the fourth degree for F_4^h and to the second degree in the ρ_i, $(d\rho_i/du)$, and $(d\Theta_i/du)$ for F_4^{inh}.

In order to work out the phase diagrams involving the transitions from the P structure to the $2H_a$ and $Cmcm$ structures one has to minimize the total free energy $\int F_t(T,P,\eta,\rho_i,\Theta_i)dV$ (summed over a given volume of the system) with

$$F_t(T,P,\eta,\rho_i,\Theta_i)dV = F_1(T,P,\eta) + F_4^h(T,P,\rho_i,\Theta_i) \times \delta\eta^2[(\rho_1^2+2\rho_2^2)+F_4^{inh}], \quad (7)$$

where F_1 is expressed by Eq. (1) and the δ term represents the coupling between the order parameters associated with the $P\rightarrow 2H_a$ and $P\rightarrow Cmcm$ transitions. Using the minimization procedure described in Ref. 29, which consists of simplifying the standard Euler-Lagrange minimization process, one can deduce the phase diagrams shown in Fig. 6. The topologies of the phase diagrams depend on the sign and magnitude of the phenomenological coefficients in the Landau free energy and on the degrees to which F_1, F_4^h, and F_4^{inh} are expanded. Figure 6(a) represents the simplest situation where the $P6_3/mmc$ and $Cmcm$ phases are separated by an incommensurate phase (INC) as it is observed experimentally in $2H_a$-$TaSe_2$ at atmospheric pressure. However the three phases are separated by second-order transitions whereas the INC-$Cmcm$ transition is experimentally first order. Figure 6(b) shows a more realistic phase diagram in which the lock-in INC-$Cmcm$ transition is of first order, whereas the $2H_a\rightarrow$INC transition can be either first or second order depending on the thermodynamic path. The phase diagram of Fig. 6(c), which assumes an eighth-degree expansion of F_4^h shows an INC phase located between two $Cmcm$ phases as it is observed in $2H_a$-$TaSe_2$ with increasing pressure.[30] The phase diagram of Fig. 6(d) implies a fourth-degree expansion in F_4^{inh} and reveals the possibility of stabilizing two distinct incommensurate phases.

A similar description of the phase diagrams resulting from the coupling between the layer stacking and in-layer transitions can be performed for the other TMD polytypes. However the corresponding symmetry and thermodynamic considerations are more complex due to the location of the relevant critical wave vectors. With the exception of the $1T$-$TiSe_2$ superstructure, which can be related to a three-dimensional IREP at the L point of the $P6/mmm$ space group $(\tau_2(\mathbf{k}_{14}))$, the superstructures found in $1T$-VSe_2, $1T$-TaS_2, and $1T$-$TaSe_2$ correspond to critical wave vectors in general positions in the ΓML plane of the hexagonal Brillouin zone (Fig. 5). It therefore coincides with a 24-dimensional IREP of the parent (or $P\bar{3}m1$) structure. For the superstructures found in the $4H_b$ and $6R$ polytypes the in-layer transitions correspond, as for the $2H_a$ polytypes, to critical wave vectors on the zone-boundary R line, but the stacking order is associated with two-component order-parameter expansions involving inhomogeneous terms. Therefore the coupling between the layer stacking and in-layer superstructures leads to a minimization procedure of the total free energy which is more difficult to handle.

IV. SUMMARY AND CONCLUSION

In summary, we have shown that the large number of polytypic structures occurring in TMD materials can be associated with different ordering mechanisms from the same parent disordered structure formed by one MX_2 subunit. This disordered polytype structure gives rise to intrinsic stacking faults in the resulting ordered polytype structures and favors the crossover between the polytypes. The coupling of the preceding ordering mechanism with the structural transitions occurring within the layers in some TMD compounds allows us to clarify some discrepancies with the two-dimensional models and allows to work out the topology of the phase diagrams of TMD materials when intrapolytypic and interpolytypic transitions are involved concurrently.

ACKNOWLEDGMENT

This work was supported by the German Science Foundation (Grant No. FOR 353, DE412/21-1,2).

*Electronic address: hanne@min.uni-kiel.de

[1] F. Jellinek, G. Brauer, and H. Müller, Nature (London) **185**, 376 (1960).
[2] *Intercalated Layered Materials*, edited by F. Lévy (Reidel, Dordrecht, 1979).
[3] *Structural Phase Transitions in Layered Transition Metal Compounds*, edited by K. Motizuki (Reidel, Dordrecht, 1986).
[4] *Charge Density Waves in Solids*, edited by L.P. Gor'kov and G. Grüner (North-Holland, Amsterdam, 1989).
[5] L.S. Ramsdell, Am. Mineral. **32**, 64 (1947).
[6] O.V. Kovalev, *Irreducible Representation of Space Groups* (Gordon and Breach, New York, 1965).
[7] J.C. Tolédano and P. Tolédano, *The Landau Theory of Phase Transitions* (World Scientific, Singapore, 1987).
[8] F. Kadijk and F. Jellinek, J. Less-Common Met. **23**, 437 (1971).
[9] M. Marezio, P.D. Dernier, A. Menth, and G.W. Hull, J. Solid State Chem. **4**, 425 (1972).
[10] F. Kadijk, R. Huisman, and F. Jellinek, J. Less-Common Met. **21**, 187 (1970).
[11] W. Geertsma, C. Haas, R. Huisman, and F. Jellinek, Solid State Commun. **10**, 75 (1972).
[12] F. Jellinek, J. Less-Common Met. **4**, 9 (1962).
[13] H. Jagodzinski, Acta Crystallogr. **7**, 300 (1954).
[14] J.A. Wilson, F.J. DiSalvo, and S. Mahajan, Adv. Phys. **24**, 117 (1975).
[15] D.E. Moncton, J.D. Axe, and F.J. DiSalvo, Phys. Rev. Lett. **34**, 734 (1975).
[16] D.E. Moncton, J.D. Axe, and F.J. DiSalvo, Phys. Rev. B **16**, 801 (1977).
[17] S. Tanda, T. Sambongi, T. Tani, and S. Tanaka, J. Phys. Soc. Jpn. **53**, 476 (1984).
[18] J. Lüdecke, S. van Smaalen, A. Spijkerman, J.L. de Boer, and G.A. Wiegers, Phys. Rev. B **59**, 6063 (1999).
[19] P.B. Littlewood and T.M. Rice, Phys. Rev. Lett. **48**, 27 (1982).
[20] T.M. Rice, Phys. Rev. B **23**, 2413 (1981).
[21] A.E. Jacobs and M.B. Walker, Phys. Rev. B **21**, 4132 (1980).
[22] W.L. McMillan, Phys. Rev. B **12**, 1187 (1975).
[23] W.L. McMillan, Phys. Rev. B **14**, 1496 (1976).

[24] M.B. Walker and A.E. Jacobs, Phys. Rev. B **25**, 4856 (1982).
[25] M.B. Walker and R.L. Withers, Phys. Rev. B **28**, 2766 (1983).
[26] K. Nakanishi and H. Shiba, J. Phys. Soc. Jpn. **53**, 1103 (1984).
[27] H. Shiba and K. Nakanishi, in *Structural Phase Transitions in Layered Transition Metal Compounds* (Ref. 3), p. 175. Ref. 3, p.175.
[28] V. Dvořák and V. Janovec, J. Phys. C **18**, 269 (1985).
[29] B. Mettout and H. Vasseur, Europhys. Lett. **54**, 168 (2001).
[30] D.B. McWhan, R.M. Fleming, D.E. Moncton, and F.J. DiSalvo, Phys. Rev. Lett. **45**, 269 (1980).